Ocean Dynamics (2016) 66:567–588
DOI 10.1007/s10236-016-0938-y

Objective assessment of the contribution of the RECOPESCA network to the monitoring of 3D coastal ocean variables in the Bay of Biscay and the English Channel

Julien Lamouroux[1,2] · Guillaume Charria[3] · Pierre De Mey[4] · Stéphane Raynaud[5] · Catherine Heyraud[5] · Philippe Craneguy[5] · Franck Dumas[6] · Matthieu Le Hénaff[7,8]

Received: 24 July 2015 / Accepted: 22 February 2016 / Published online: 11 March 2016
© Springer-Verlag Berlin Heidelberg 2016

Abstract In the Bay of Biscay and the English Channel, in situ observations represent a key element to monitor and to understand the wide range of processes in the coastal ocean and their direct impacts on human activities. An efficient way to measure the hydrological content of the water column over the main part of the continental shelf is to consider ships of opportunity as the surface to cover is wide and could be far from the coast. In the French observation strategy, the RECOPESCA programme, as a component of the High frequency Observation network for the environment in coastal SEAs (HOSEA), aims to collect environmental observations from sensors attached to fishing nets. In the present study, we assess that network using the Array Modes (ArM) method (a stochastic implementation of Le Hénaff et al. Ocean Dyn 59: 3–20. doi: 10.1007/s10236-008-0144-7, 2009). That model ensemble-based method is used here to compare model and observation errors and to quantitatively evaluate the performance of the observation network at detecting prior (model) uncertainties, based on hypotheses on error sources. A reference network, based on fishing vessel observations in 2008, is assessed using that method. Considering the various seasons, we show the efficiency of the network at detecting the main model uncertainties. Moreover, three scenarios, based on the reference network, a denser network in 2010 and a fictive network aggregated from a pluri-annual collection of profiles, are also analysed. Our sensitivity study shows the importance of the profile positions with respect to the sheer number of profiles for ensuring the ability of the network to describe the main error modes. More generally, we demonstrate the capacity of this method, with a low computational cost, to assess and to design new in situ observation networks.

Keywords Design of in situ observation network · Bay of Biscay · English Channel · Performance assessment · Model errors

Responsible Editor: Emil Vassilev Stanev

This article is part of the Topical Collection on *Coastal Ocean Forecasting Science supported by the GODAE OceanView Coastal Oceans and Shelf Seas Task Team (COSS-TT)*

✉ Guillaume Charria
Guillaume.Charria@ifremer.fr

Julien Lamouroux
Julien.Lamouroux@mercator-ocean.fr

[1] NOVELTIS, 153 rue du Lac, 31670 Labège, France

[2] Mercator-Océan, 8-10 rue Hermès, 31520 Ramonville Saint-Agne, France

[3] Ifremer, Univ. Brest, CNRS, IRD, Laboratoire d'Océanographie Physique et Spatiale (LOPS), IUEM, F-29280 Brest, France

[4] CNRS, LEGOS/UMR 5566, 18, av. Edouard Belin, 31401 Toulouse, Cedex 9, France

[5] ACTIMAR, 36, quai de la Douane, 29200 Brest, France

[6] SHOM, HOM, 13 Rue de Châtellier, 29200 Brest, France

[7] University of Miami/Cooperative Institute for Marine and Atmospheric Studies (CIMAS), 4600 Rickenbacker Causeway, Miami, FL 33149-1098, USA

[8] NOAA Atlantic Oceanographic and Meteorological Laboratory (AOML), 4301 Rickenbacker Causeway, Miami, FL33149, USA

1 Introduction

The extent and quality of coastal observing systems have been fluctuating with improvements of sensors and platforms, and with the availability of dedicated funding. Despite the small number of regions with sustained coastal observations, the infrastructures for coastal environment monitoring represent

a significant contribution to the Global Ocean Observing Systems. Indeed, close to the coast, the amount of needed observations increases due to the wide range of spatial and temporal scales to monitor (e.g. tide impact, river plumes, exchanges between open and coastal ocean) and their direct impacts on human activities. In addition, coastal ocean monitoring is becoming a major goal for public authorities in an effort to predict and mitigate various types of events. However, since a wide use of satellite data is limited in coastal areas (due for instance to lack in time repetitivity or to the presence of the coast in the case of altimetry measurements), in situ (e.g. moorings, gliders) or short range remotely sensed data (e.g. HF Radar) are then the most reliable source of information. Let us also cite the need for integrated approaches, optimally and synoptically combining undersampled and fragmented observations with models to monitor coastal ocean features and their evolutions.

The usual approach to design and optimize these networks is to consider our knowledge from the regions of deployment and the processes driving the dynamics in this area. Since the aim is to objectively define the best network in a region generally only partially known, numerical models usually play an important role in the approaches. One can decide to assimilate virtual data from the targeted observing system in the framework of the so-called OSSE ("Observing System Simulation Experiment") approach (e.g. Alvarez and Mourre 2014; Lea et al. 2014; Halliwell et al. 2014) and analyse how much of the model errors are constrained. However, this valuable method is computationally expensive and depends on whether an agreed-upon data assimilation system already exists in the considered region. A recent method (Le Hénaff et al. 2009), retained for this study and based on stochastic modelling, allows exploring a wide range of networks for different time periods. Based on a notion akin to the array modes as defined by Bennett (1985, 1990), the so-called ArM (Array Modes) methodology can be applied to evaluate the objective performance of a network design at detecting prior errors without having to run a fully assimilated system.

The aim of the present study is to assess the performance of an existing and highly time-varying in situ network in the Bay of Biscay and the English Channel (Fig. 1a). This network—RECOPESCA (Leblond et al. 2010)—is based on opportunity fishing vessels with fishing nets instrumented using temperature, salinity, pressure and some turbidity sensors. Regions of deployment (Bay of Biscay and English Channel) are located in the eastern part of the North Atlantic Ocean between the Spanish, French, British and Irish coasts. RECOPESCA is a component of the High frequency Observation network for the environment in coastal SEAs (HOSEA) operated by IFREMER (Institut Francais de Recherche Pour l'Exploitation de La MER—French Research Institute for Exploitation of the Sea). The irregular and steep bathymetry in this region (narrow 30 km continental shelf in the South, wide 180 km shelf off Brittany) combined with the seasonality wind regimes (Isemer and Hasse

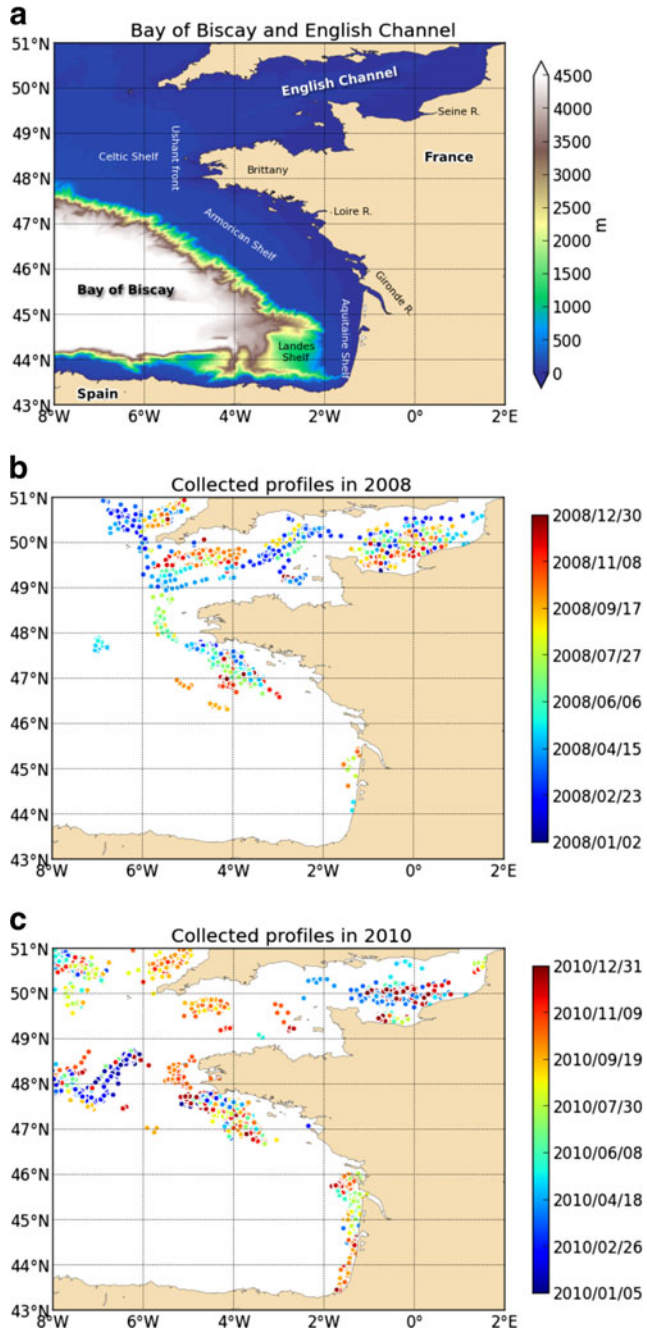

Fig. 1 **a** Map and bathymetry of the Bay of Biscay and the English Channel (Seine R., Loire R. and Gironde R. are rivers). **b**, **c** RECOPESCA profiles collected in 2008 and 2010 as a colour-coded function of time of year

1985; Pingree and Le Cann 1989, 1990) and significant, season-related river discharges (e.g. Ferrer et al. 2009; Lazure and Jégou 1998; Lazure et al. 2006) drives a wide range of processes (e.g. slope currents, mesoscale eddies, shelf circulation—Charria et al. 2013) interacting in a region strongly influenced by tides (e.g. Pichon and Correard 2006; Pairaud et al. 2008, 2010). Over the continental shelf in the Bay of Biscay, the dynamics is mainly driven by barotropic tides dominant in the northern part of the

domain and density gradients mainly driven by river plumes with regions of freshwater influence spreading over most of the shelf in the winter. Clearly, the locations visited by the fishing fleet only allow to capture part of those processes, depending on the time of year, but also on external factors such as weather conditions and stock management.

The paper is organized as follows: the RECOPESCA network, in a reference configuration, as well as for some extension scenarios, is described in Section 1; Section 2 is dedicated to a brief description of the ArM methodology formalism. The performance analyses for the reference network and for the extended scenarios, respectively, are discussed in Sections 4 and 5, and conclusions are drawn in Section 6.

2 RECOPESCA network

The RECOPESCA project provides an observation network, based on voluntary vessels, of the fisheries activity (effort and catches) and the environment. These measurements contribute to the evaluation of exploited resources and to the collection of new environmental data, as water temperature, salinity and turbidity (oxygen and fluorescence sensors are under development). Since 2007, the system has been widely deployed on an increasing number of voluntary vessels after a test period initiated in 2006. Specific sensors are implemented on the fishing gears and aboard a sample of vessels representative of the whole fishing fleets. These sensors have been developed to be suitable for conditions and constraints aboard fishing vessels (tough enough to be fixed up on fishing gears, self powered, autonomous, affordable, able to run without any intervention of the fishermen neither causing trouble for their fishing activity). The time of the nets in water can be variable. However, the position of the vertical profiles is synchronized with the ship's position when the sensor is close enough to the station on board, and then it remains independent of the time of the net under water. For the time spent in the lower water column, another product (not used in the present study) is existing, called Time Series, which is representing a time series of measurements at depth. This product is particularly interesting when the probes are fixed on crab boat traps.

In the present study, we are focusing on sensors for physical environmental data profiling temperature, pressure, salinity and turbidity. Data are collected at the bottom and along the water column. They are transmitted to a data station on board before sending measurements to main databases on land via the GPRS network when available. This data flux is then close to real time (depending the GPRS network and following the automatic qualification), and it allows monitoring the hydrological structures with a vertical sampling around 0.2 m. Figure 1 displays the positions of profiles collected in 2008 (Fig. 1b) and 2010 (Fig. 1c). During these years, the number of valid profiles was increasing with 2395 profiles in 2008, 3388 profiles in 2009 and 5317 profiles in 2010 to reach 6756 profiles in 2013 and 4760 profiles in 2014. Thirty-three thousand two hundred seventy-six profiles have been collected between 2006 and 2014. Following targeted fishing areas, profiles are mainly located south of Brittany, in the Celtic Sea and in the English Channel in 2008 (Fig. 1b). In 2010, an increase in the number of collected profiles is observed with an extent of the areas covered by equipped fishing vessels. Indeed, data along the southwest French coast have been collected as well as new data further offshore in the Celtic Sea (Fig. 1c). The time of the nets in water can be variable. However, the position of the profile is synchronized with the ship's position when the sensor is close enough to the station on board, and then it remains independent of the time of the net under water. For the time spent at depth, there is another product (not used in the present study), called Time Series, which is representing a time series of the measurements at depth. This product is particularly interesting when the probes are fixed on crab boat traps.

The spatial and temporal distribution of RECOPESCA profiles allows exploring the main features of the vertical hydrological structures and their variability (Leblond et al. 2010; Charria et al. 2014). Indeed, large number of profiles, south of Brittany, allows highlighting interannual evolutions in temperature since 2007 (Charria et al. 2014). Further investigations are in progress to extend this analysis in salinity and in other subregions in the Bay of Biscay and the English Channel.

3 Methodology

3.1 Towards a criterion of array performance

In the following, we will use the following paradigm: a "good" array, regardless of its cost, is an array that can detect—and help correct—errors of a prior (i.e. pre-existing) estimate. This estimate can be from a model, a climatology or a null estimate if nothing is known beforehand.

A variant of our approach has been described in detail by Le Hénaff et al. (2009); it will be recalled briefly below. For the calculations carried out in this paper, we will adopt a formalism (hereafter ArM) based on the very same idea, but where the stochastic nature of error estimates is explicitly taken into account (De Mey 2014, personal communication, implemented and available in the SANGOMA Tools http://www.data-assimilation.net/Tools/). Although no data assimilation will be carried out here, we will use the unified notations of data assimilation as in Ide et al. (1997).

Let us define x, an augmented state vector of dimension n over the time interval of interest (it can be noticed that this is

an *augmented* state vector—everything that will be shown below includes time as well as space in the definition of observations and prior state estimate). n is of the order of 1.7×10^7 in our case of study.

Let us define $\mathbf{y}^o$, the vector of observations of dimension p verifying $\mathbf{y}^o = H(\mathbf{x}^t) + \varepsilon$, with $\mathbf{x}^t$ the "true" state, $H(\,)$ an observation operator (not necessarily linear, but for the sake of clarity we will use a linearized operator $\mathbf{H}$), and Gaussian measurement error $\varepsilon \in N(0, \mathbf{R})$, with $\mathbf{R}$ being the observational *Error Covariance Matrix* (hereafter ECM). p is of the order of 1×10^5 in our case of study.

Our question is the following: how can we characterize the performance of an observational array as defined by (H, $\mathbf{R}$) in such a way that we can compare the performance of one array to another?

Let us assume that we have a prior estimate of x and of its associated error statistics (if not, any observational array will bring valuable information proportionately to its cost), i.e. $\mathbf{x}^f = \mathbf{x}^t + \eta$, with $\eta \in N(0, \mathbf{P}^f)$, $\mathbf{P}^f$ being an estimate of the prior ECM (we will come back later to how we can get such an estimate). ε and η are assumed to be independent random vectors.

Let us consider the incremental "information" brought in by the array on top of the prior. (Part of this is new information, but part is noise.) To do that, we introduce the *innovation vector* and its second-order statistics:

$$\mathbf{d} \equiv \mathbf{y}^o - \mathbf{y}^f = \mathbf{y}^o - H\left(\mathbf{x}^f\right) = H(\mathbf{x}^t) + \varepsilon - H(\mathbf{x}^t + \eta) \approx \varepsilon - \mathbf{H}\eta. \quad (1)$$

$$\left\langle \mathbf{d}\mathbf{d}^T \right\rangle = \mathbf{R} + \mathbf{H}\mathbf{P}^f\mathbf{H}^T. \quad (2)$$

We reach a coarse but intuitive "global" criterion of array performance:

- If observational errors ($\mathbf{R}$) dominate in Eq. (2), then most of the discrepancies are attributable to observational error, and observations are not being very useful.
- If prior state errors ($\mathbf{H}\mathbf{P}^f\mathbf{H}^T$), commonly called *Representer Matrix* (hereafter RM) dominate, then most of the discrepancies are attributable to prior state errors, and observations can be expected to be useful at identifying and correcting the prior state errors.

We now endeavour to formalize that global criterion so that we can use it to compare whole arrays to each other. Le Hénaff et al. (2009) do this by first projecting Eq. (2) and the RM onto a space where the observational ECM becomes diagonal:

$$\begin{aligned} &\mathbf{R}^{-1/2}\left\langle \mathbf{d}\mathbf{d}^T \right\rangle \mathbf{R}^{-1/2} = \mathbf{I} + \chi \\ &\chi = \mathbf{R}^{-1/2}\mathbf{H}\mathbf{P}^f\mathbf{H}^T\mathbf{R}^{-1/2} \end{aligned}. \quad (3)$$

In a second step, they formalize the above criterion by comparing the eigenspectrum $\boldsymbol{\sigma}$ of χ to the eigenspectrum of $\mathbf{I}$, which is trivial and equal to 1. The eigenvectors $\boldsymbol{\mu}$ of the projected RM χ are called *array modes*:

$$\chi = \boldsymbol{\mu}\boldsymbol{\sigma}\boldsymbol{\mu}^T. \quad (4)$$

Therefore, in first instance, the intuitive criterion above comes back to counting how many eigenvalues in Eq. (4) lie above 1. The corresponding array modes will be the "detectable" error modes above the observational noise floor. Note that the observational ECM does not need to be diagonal: correlated errors can be considered as shown in Le Hénaff et al. (2009). The number of eigenvalues above 1 can be used to compare whole arrays to each other; this should however be completed by the examination of array modes, since the error degrees of freedom detected by two very different arrays can also widely differ in nature.

Extending the classic notion of *representers* (the influence functions of individual observations), Le Hénaff et al. (2009) also introduce *modal representers*, which project array modes onto the state (physical) space and can be used to examine the theoretical correction which would be applied by a particular array mode if assimilation took place in a further step:

$$\boldsymbol{\rho}_\mu = \mathbf{P}^f\mathbf{H}^T\mathbf{R}^{-1/2}\boldsymbol{\mu}. \quad (5)$$

3.2 Stochastic implementation

Let us now assume that we have a way of generating m realistic prior error samples, e.g. from stochastic modelling or an ensemble filter. By "realistic", we mean that we believe that these samples are indeed representatives of the errors of our prior estimate. In Le Hénaff et al., the χ matrix was also calculated from ensemble statistics using pre-calculated ensemble members. However, here, we wish to directly take into account the stochastic generation of prior errors in the formalism. What is described below is the version of the ArM algorithm which is available in the SANGOMA tools.

Let us define our generator—a matrix of m-centred error samples, $\mathbf{A}^f$, of dimension $n \times m$. The prior ECM is approximated from the samples as $\hat{\mathbf{P}}^f = \frac{1}{m-1}\mathbf{A}^f\mathbf{A}^{f^T}$. The projected RM χ is approximated by:

$$\hat{\chi} = \frac{1}{m-1}\left(\mathbf{R}^{-1/2}\mathbf{H}\mathbf{A}^f\right)\left(\mathbf{R}^{-1/2}\mathbf{H}\mathbf{A}^f\right)^T = \mathbf{S}\mathbf{S}^T \quad (6)$$

where $\mathbf{S} = \frac{1}{\sqrt{m-1}}\mathbf{R}^{-1/2}\mathbf{H}\mathbf{A}^f$ contains the scaled ensemble observation anomalies (this is the same $\mathbf{S}$ matrix as in Sakov et al. 2010). From Eq. (6), it follows that the eigenvalue problem Eq. (4) can now be expressed as a singular value problem:

- The eigenspectrum $\boldsymbol{\sigma}$ is estimated as the square of the singular value spectrum of $\mathbf{S}$.

- The array mode estimates $\hat{\boldsymbol{\mu}}$ are the singular vectors of $\mathbf{S}$.
- The modal representer estimates are $\hat{\boldsymbol{\rho}}_{\mu} = \frac{1}{\sqrt{m-1}}\mathbf{A}\mathbf{S}^T\hat{\boldsymbol{\mu}}$.

3.3 Stochastic modelling

The stochastic generator described above can for instance be built by randomly perturbing the error sources of the model (e.g. Auclair et al. 2003; Mourre et al. 2004; Mourre and Ballabrera-Poy 2009).

Here, we used an ensemble of 50 perturbed simulations with the MARS3D model (Lazure and Dumas 2008; Duhaut et al. 2008) generated as a combined response to the following sources of errors:

- Uncertainties in the atmospheric forcings, which have been modelled through a dynamical 50-member ensemble of Gaussian-perturbed atmospheric fields (pressure at sea level, 10 m-wind, surface heat fluxes, 2 m-temperature) provided by ECMWF (Buizza 2006);
- Uncertainties in specific model parameters, namely the bottom friction coefficient, the turbulent-closure coefficient and the light-extinction coefficient, which were slightly perturbed following a Gaussian distribution. Those parameters were retained since they have been shown to have a significant impact on the model results and are—at least—partly uncorrelated (Friedrichs 2001; Huret et al. 2007).

The MARS3D model configuration is running with a 4-km spatial resolution and 40 sigma vertical levels. The resulting ensemble has been generated for the year 2006. As described in Section 3.2, we considered anomalies with respect to the ensemble mean. Figure 2 illustrates the statistical consistency of the ensemble over the spring period, which has been first assessed against hourly sea surface temperature (SST) fields, derived from the Spinning Enhanced Visible and Infrared Imager (SEVIRI) onboard Meteosat Second Generation (MSG) (EUMETSAT 2006).

First, it can be stated from Fig. 2a, b that the ensemble mean is statistically very similar to the unperturbed reference simulation. This is an indication that the resulting ensemble distributions—and the associated model error structures—are close to a Gaussian distribution. However, as it has been discussed by Quattrocchi et al. (2014), investigating statistical moments of orders 1 to 4, departures from linear/Gaussian response to perturbations are likely in ensemble simulations. In the present study, this Gaussian property for the ensemble distribution is not necessary. Secondly, one can note that the model-observation deviations (Fig. 2a, b) are globally coherent with the model error structures as "seen" by the observations (Fig. 2c), for instance in front of Loire river and on Aquitaine Shelf. Local discrepancies are nevertheless visible (e.g. in western English Channel). Eventually, Fig. 2d gives an insight into the mean spatial distribution of the SST model error structures. Those structures are mainly localized on the Biscay Shelf and in the vicinity of the river estuaries, with an amplitude of the order of 0.3 °C. They a priori correspond to the signature of the atmospheric forcing, the turbulent-closure coefficient and the light-extinction coefficient uncertainties. Some error structures are also noticeable in the western English Channel and are associated with the Ushant thermal front (thermal tidal front located west of Brittany during stratified seasons, Le Boyer et al. 2009) dynamics. These error developments are probably caused by the perturbations of the bottom-friction coefficient, which indeed influenced the mixing of the water column, and the closure-turbulence coefficient. It is also likely that the atmospheric forcing perturbations have an impact on the mixing of the water column in the area and then on the generation of the error growth in the vicinity of the Ushant thermal front. As a general remark, the discrepancies that are noticeable between Fig. 2c and d illustrate the importance of the spatiotemporal measurement sampling in the specific problem of model error observability.

The average bias between simulation and observation (not shown—on average −0.11 °C in spring) does not impact the ArM method as the analysis aims to detect the efficiency of the observing system to detect and/or to constrain the system variability (using for example an ensemble variance).

3.4 Observation error

The ArM method requires an estimate of the observational ECM. Observational error is classically defined from the sum of two contributions: the measurement error, related to the sensor accuracy, and the representativity error, which is usually the result of small scale information in observations being incorrectly represented in the model, or due to the sampling protocol.

The accuracy of the autonomous temperature data logger (STPS probes developed by NKE Instrumentation[1]) is equal to 0.05 °C. We have no information as to whether the measurement error might be correlated with time and/or space.

Regarding the representativity error, we estimate that 0.25 °C is a realistic magnitude. Indeed, one can assume that this error term is representing the uncertainty in the observation linked to the sampling with regard to the targeted processes. In the present case, it will be mainly related to the position of the profile. In a macrotidal region, currents can be intense and variable, and depending on the length of the fishing net, the profile position, given by the ship position, can be inaccurate. Then, close to the thermocline depth, temperature gradients can have

[1] http://www.nke-instrumentation.com/oceanography/data-loggers/multipameter-probesfa4d.html

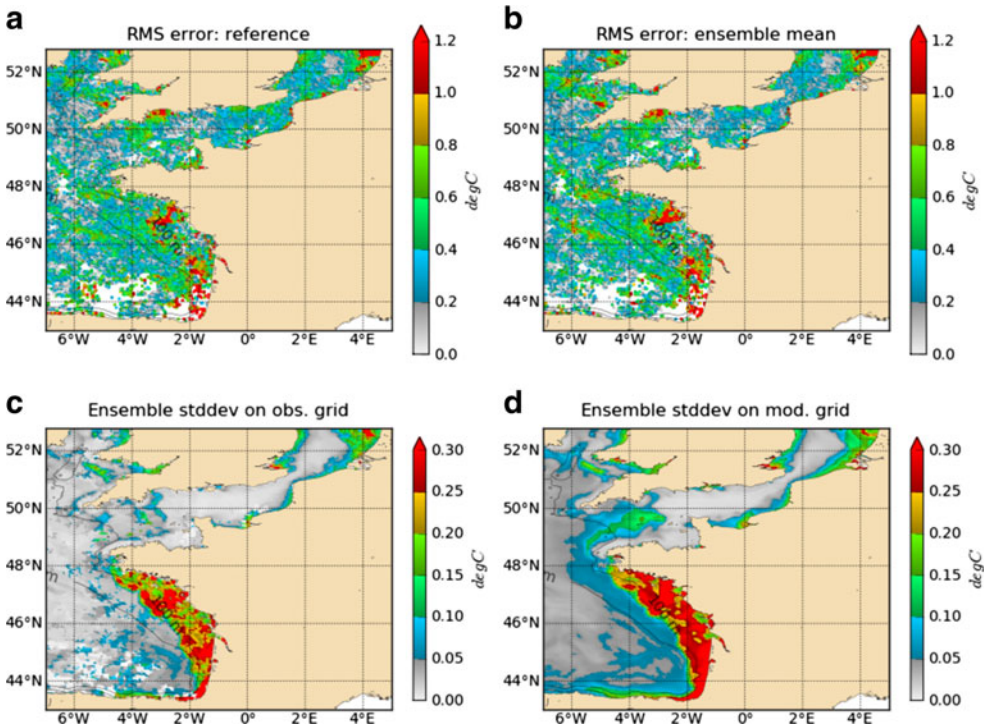

Fig. 2 Statistical consistency of the SST ensemble modelling in May 2006. **a** Temporal RMS error of the reference simulation (i.e. no perturbation applied) with regard to SEVIRI SST observations. **b** Temporal RMS error of the ensemble mean with regard to SEVIRI SST observations. **c** Time-averaged ensemble standard deviation computed on the SEVIRI observation grid. **d** Time-averaged ensemble standard deviation computed on the model grid

a large spatiotemporal variability. For example, at a given depth and a given position, temperature variations can be larger than 2 °C during few minutes of measurements (Cuypers et al. 2011). In another example close to shelf break (Xie et al. 2013), temperature variations close to the thermocline are similar. Considering these variations, 0.25 °C appears as a reasonable representativity error estimate in the studied region.

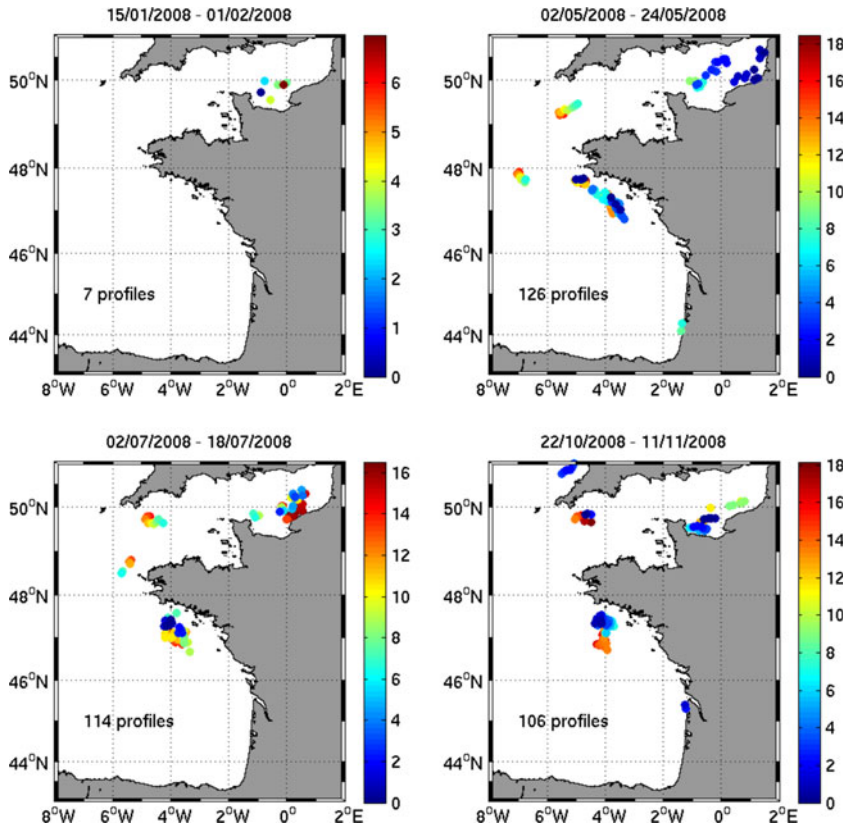

Fig. 3 Location of RECOPESCA profiles relative to the four studied periods—units: elapsed days since the first day of each period

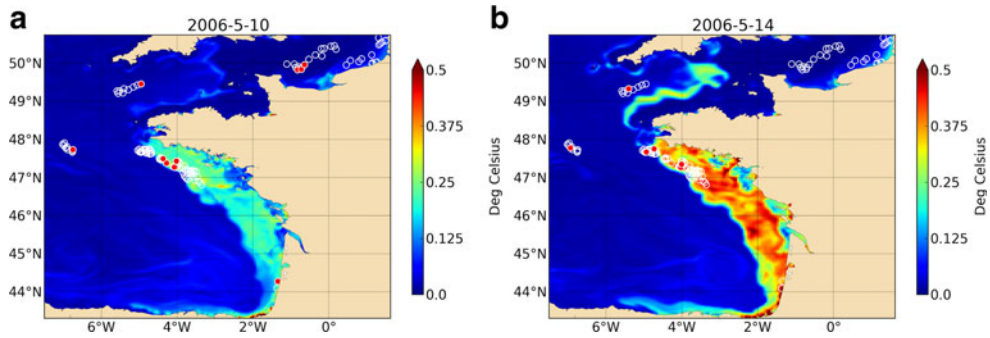

Fig. 4 Model sea surface temperature ensemble standard deviation (unit: °C) for (**a**) May 10 and (**b**) May 14, 2006 (*horizontal section* at 6 m depth). Location of available profiles during the whole period (*white circles*) and at the current date (*red spots*)

For the present study, given the above, a diagonal ECM with temperature error standard deviation equal to 0.3 °C has been chosen.

4 Assessment of the reference network

4.1 Introduction

A "reference" configuration of the RECOPESCA network has been studied during four-time periods in 2006, representative of the seasonal variability in the Bay of Biscay and the English Channel:

- January 16–February 2: winter period
- May 3–May 25: spring
- July 4–July 18: summer
- October 23–November 12: autumn

For these periods, we consider the locations of the 2008 temperature measurements (as it is the first year with a significant number of RECOPESCA observations) for testing the ability of the equivalent network to detect model error modes from the simulation runs. As a reminder, the ArM methodology only requires the locations and ECM of the observations, not the sampled measurements. These four sets of profiles are displayed in Fig. 3. The number of profiles ranges from 106 profiles (in autumn) to 126 profiles (in spring) except in the winter with very few profiles considered (only 7 profiles). Note that the distribution in time between the four seasons of the profile range has been improved during recent years.

For each period, a common analysis protocol has been applied:

1. First, an analysis of the MARS3D model error subspace is performed: the ensemble standard deviation—as a proxy of the model error–is computed over the ensemble of 50 perturbed simulations, and over the whole period. The main space-time features of this model error proxy are highlighted, with a possible focus on areas of interest.
2. This model error proxy is then interpolated (in space and time) at the profile locations, in order to give an insight into the model errors projected into the observational space. As a first approximation, the observations located where the model error is larger than 0.3 °C should be efficient in terms of detecting the model error structures.
3. ArM analysis: Performances of the RECOPESCA network are then analysed, in terms of detection of the degrees of freedom (hereafter d.o.f.) of the model error subspace: the array modes and associated spectrum, as well as modal representers (cf. Section 3.2), are computed and detailed, with a focus on subareas of interest.

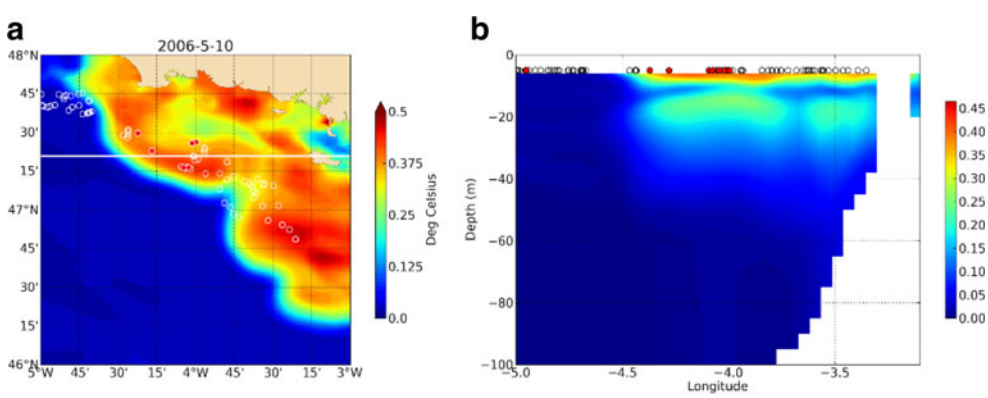

Fig. 5 **a** Six-meter depth horizontal section of the model temperature ensemble standard deviation (unit: °C) for May 10, 2006, over the Armorican shelf. The *white dashed line* indicates the position of the vertical section. **b** Corresponding East-West vertical section at 47.35° N of model ensemble variance. Location of the available profiles on the whole period (*white circles*) and at the current date (*red spots*)

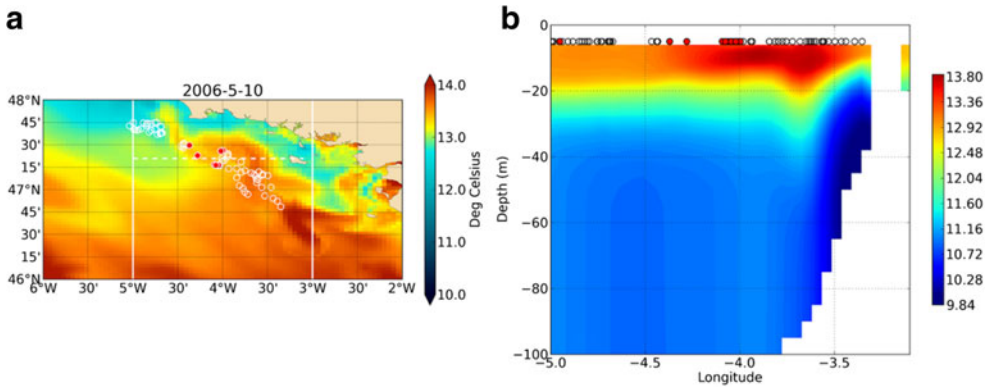

Fig. 6 (**a**) Six-meter depth horizontal section and (**b**) 47.35° N West-East vertical section of the reference temperature field, for May 10, 2006. The *white dashed line* indicates the position of the vertical section. The *white vertical line* in (**a**) indicates the box plotted in Fig. 5a. Location of the available profiles during the whole period (*white circles*) and at the current date (*red spots*)

4. The locations of the profiles with the most significant signature in the detected array modes are identified. Given a detected array mode, these profiles are associated with at least one value in the vertical which is larger than one standard deviation of all values in the array mode. By construction, these profiles shall have the most significant signature in the corresponding modal representer structure; moreover, these

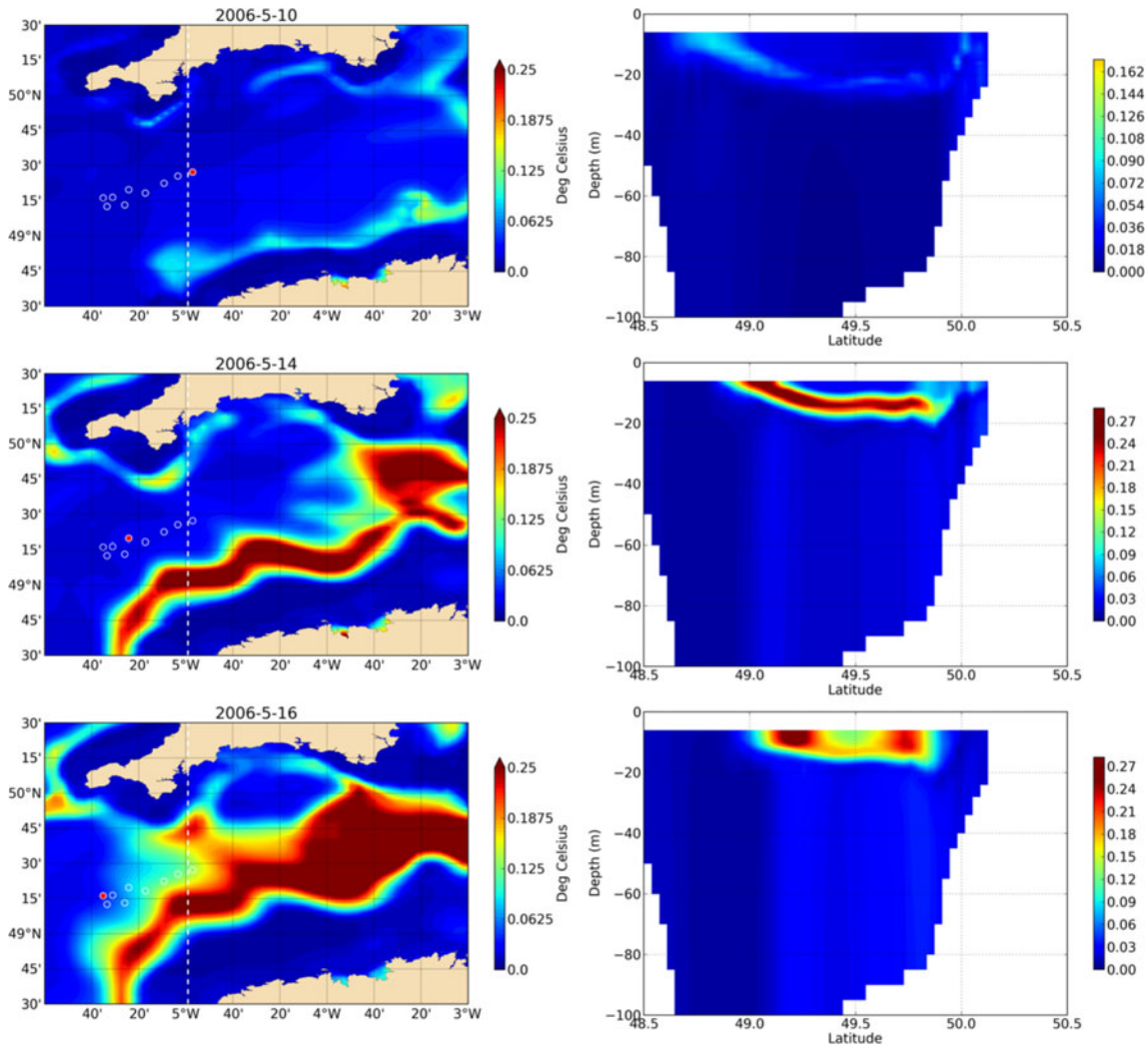

Fig. 7 *Left column*: time evolution of the 6-m depth horizontal section of the model temperature ensemble standard deviation (unit: °C) from May 10 to 16, 2006, on western English Channel. The *white dashed line* indicates the position of the vertical section. *Right column*: corresponding North-South vertical section at 5° W of model ensemble standard deviation. Location of the available profiles on the whole period (*white circles*) and at the current date (*red spot*)

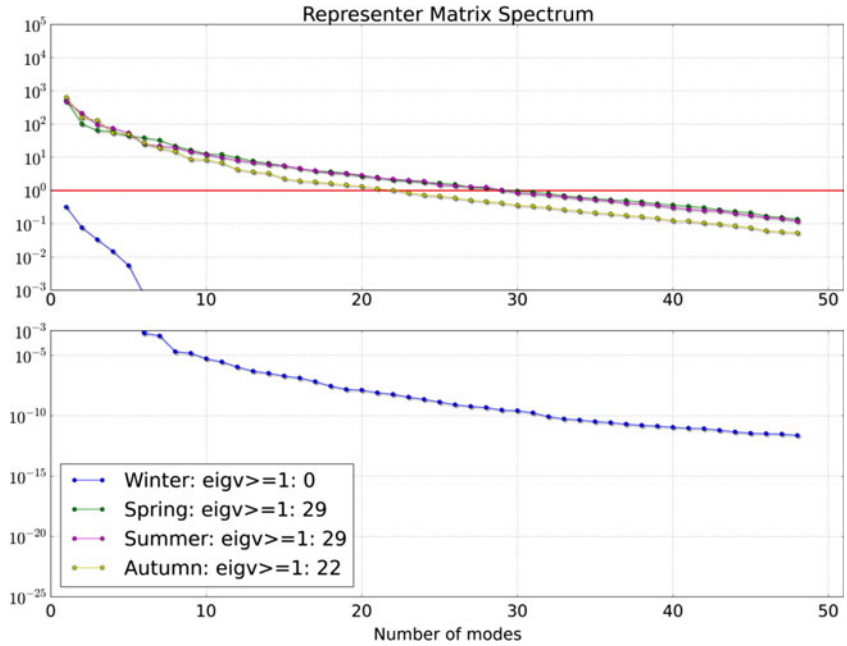

Fig. 8 Representer matrix spectra relative to the four periods: winter, spring, summer and autumn. The *top figure* is representing a zoomed spectrum for values between 10^{-3} and 10^{5}, and the *bottom figure* is the second part of the spectrum for small values (between 10^{-25} and 10^{-3}) covering a larger range of values. Spring (*green*) and summer (*purple*) curves are very close and overlap for most of the modes

profiles capture, by definition, the most "detectable" model error mode structures above the observational noise floor. Therefore, they would potentially have the most significant impact, in terms of model correction, if they were assimilated in the presence of discrepancies between their sampled measurements and the equivalent model proxy. These profiles are then called "modal profiles" in the following sections.

From this notion of modal profiles, we define an additional diagnostic for the discrimination of various RECOPESCA configurations, with the aim of proposing an objective notion of efficiency for a given RECOPESCA array. Such an efficiency indicator is defined as the ratio $e_f = \frac{n_{MP}}{n_P}$ of n_{MP}, the population of modal profiles, to n_P, the whole population of available profiles. This indicator is of particular interest for the analysis of the RECOPESCA extension scenarios, which are based on a collection of several years of profile sampling (cf. Section 5.2).

4.2 Detailed description of the spring season

Following the model error distribution—characterized by larger ensemble variance in spring and summer—and the availability of in situ profiles—which is higher during spring—the spring conditions have been put under focus for this assessment experiment of the RECOPESCA network. These spring conditions are thus fully detailed in the following sections. Other seasons are shortly described in Section 4.3.

4.2.1 Model error subspace

During the spring season, the modelled error structures (Fig. 4) are mainly located over the Armorican and Aquitaine shelves, in the eastern part of the northern Spanish coast, as well as in the vicinity of the Ushant thermal front.

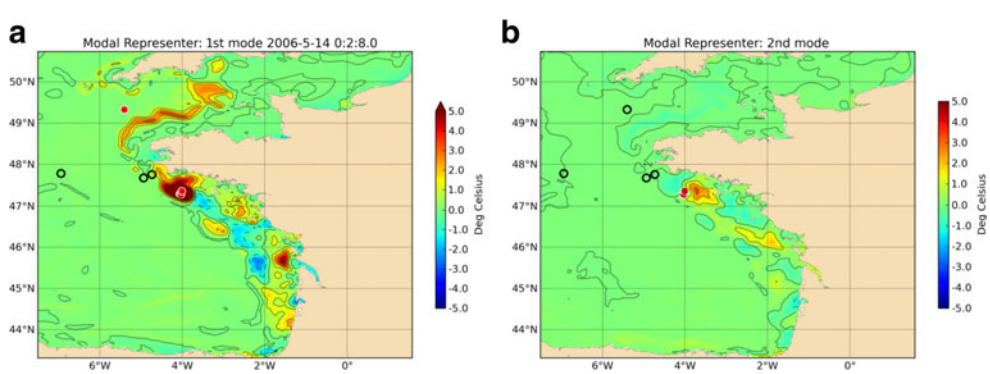

Fig. 9 First (**a**) and second (**b**) modal representers (6-m-depth horizontal section) for May 14, 2006 (unit: °C). Location of the profiles (*black circles*) and the modal profiles (*red spots*) at this date

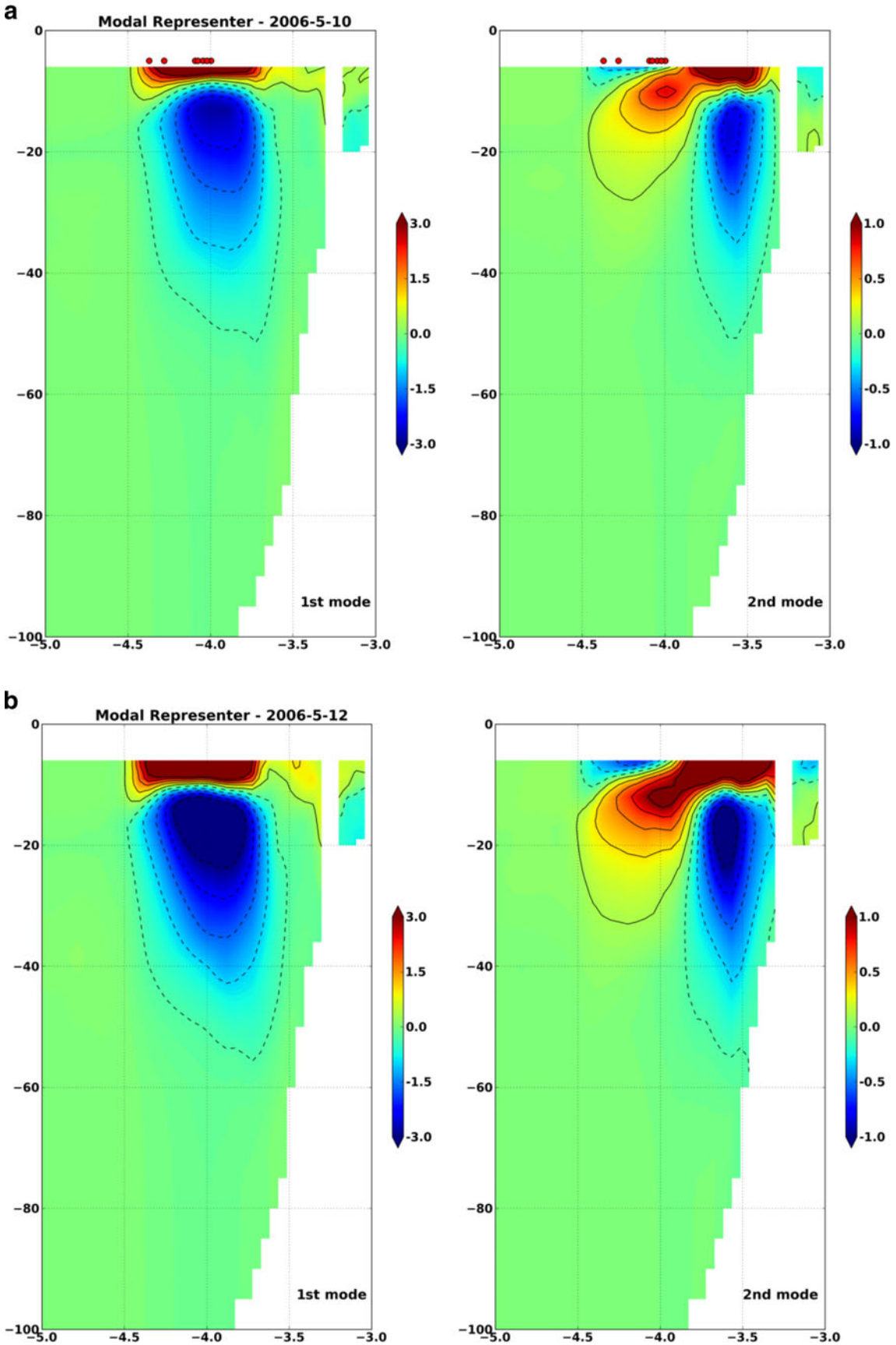
a
Modal Representer - 2006-5-10
1st mode
2nd mode
b
Modal Representer - 2006-5-12
1st mode
2nd mode

◀ **Fig. 10** East-West vertical section of the first and second modal representers for (**a**) 10, (**b**) 12, (**c**) 14, and (**d**) 16 May 2006, at 47.4° N on the Armorican shelf (unit: °C)

The model uncertainties over the Bay of Biscay shelf are mainly located in regions under freshwater influence (mainly Loire and Gironde rivers) and have been shown to be generated by the perturbations of atmospheric forcings and extinction coefficient (Heyraud et al. 2011). In the vicinity of the Ushant front, these model errors are mainly generated by the perturbations of bottom-friction and turbulence-closure coefficients.

During this period, a total of 126 profiles is available and can be gathered in four subsets (Fig. 3). A first one is located in the eastern part of the English Channel, where profiles are mainly sampled at the very beginning of the measurement period. In this area, the model errors remain very low (under 0.05 °C), so that this first group of profiles does not sample any significant model error structures. A second set of profiles is located in the western part of the English Channel, mostly in the middle and at the end of the measurement period. This set of profiles provides an efficient sampling of the model error structures in the area of the Ushant thermal front. A third group of sample profiles is located on the Armorican shelf and almost covers the whole period. Due to their wide space-time coverage, these profiles provide an efficient detection of the model error structures that develop in this area. The last set of profiles is localized above the Armorican shelf slope and does not sample significant model error structures. Consequently, considering the capability of the network to sample the model errors during this period, a focus is set on the Armorican shelf and on the western English Channel during the period from May 10 to 16, 2006.

Figure 5 shows the development, on the Armorican Shelf, of an error cell that mainly extends in the inner shelf above 40 m depth. Maximum values, larger than 0.3 °C, are mainly located in the first 10 m, but a second local maximum is reached around 20 m depth. This error cell is associated with a warming of the upper water-column in the area, inducing a deepening of the thermocline (Fig. 6); this error structure is thus thought to be mainly related to the perturbations of the light penetration and atmospheric forcings in the area. A significant number of profiles are adequately scattered in this error cell: from May 10 to 16, 2006, 27 profiles could potentially provide an efficient sampling of the error structure (see red dots in Fig. 5 for May 10, 2006).

In the western English Channel, an error cell is observed to extend horizontally and vertically in the vicinity of the Ushant thermal front (Fig. 7—north-west of Brittany). During this period, the error structure, shaped like an East-West horizontal layer, rises up to the surface. The vertical extension varies between 10 and 20 m depth, with maximum values around 0.3 °C. From May 10 to 16, 2006, several profiles are localized in the error structure and will be shown to have a significant impact on its detection by the associated network.

4.2.2 ArM analysis

In this section, the array modes and the associated spectrum, as well as the modal representers, are explored to assess the performances of the reference network to detect the model error structures previously described in Section 4.2.1.

During this spring period, the profile population of the reference RECOPESCA network is adequately scattered in time and space and is then able to detect 29 d.o.f. of the model error subspace (Fig. 8), amongst the 50 detectable d.o.f. (the rank of the system is imposed by the dimension of the ensemble of perturbed simulations, i.e. 50). The first and second modes are dominant, explaining more than 51 and 10 % of the system variance. Moreover, in both areas under focus, the first and second modal representers provide an efficient description of the main model error structures:

1. On Armorican shelf, the time development of the error cell both in horizontal and vertical dimensions is well described by the first and second representers. The first one is able to reproduce the vertical two-layer structure of the error cell, and the second one brings some refinements in this vertical structure, especially towards the coast (Fig. 10).
2. In the western English Channel, both representers provide a satisfying description of the space-time development of error structures associated with the Ushant thermal front perturbations: the error structure, shaped like an East-West horizontal layer, is efficiently detected by one modal profile associated with the first representer. The second representer, while associated with no modal profile in the western English Channel, also provides a satisfying description of the Ushant thermal front error structure. In particular, both representers are able to reproduce the rise of the error layer up to the surface (Fig. 11).

Also note that the efficiency indicator e_f (cf. Section 4.1), associated with the first and second modal representers, can reach significant level: for instance, on May 14, 2006, the first and second modal representers are associated with, respectively, five and four modal profiles, amongst the whole eight profiles available for this date (Fig. 9); this leads to efficiency values of, respectively, 0.625 and 0.5, reflecting a significant efficiency of the network at that particular time.

Therefore, the RECOPESCA network, in its reference configuration, is shown to provide an efficient detection (29 modal profiles for the first modal representer over 126 profiles—$e_f = 29/126 = 0.23$) of the model error subspace d.o.f. during the period from May 3 to 25, 2006.

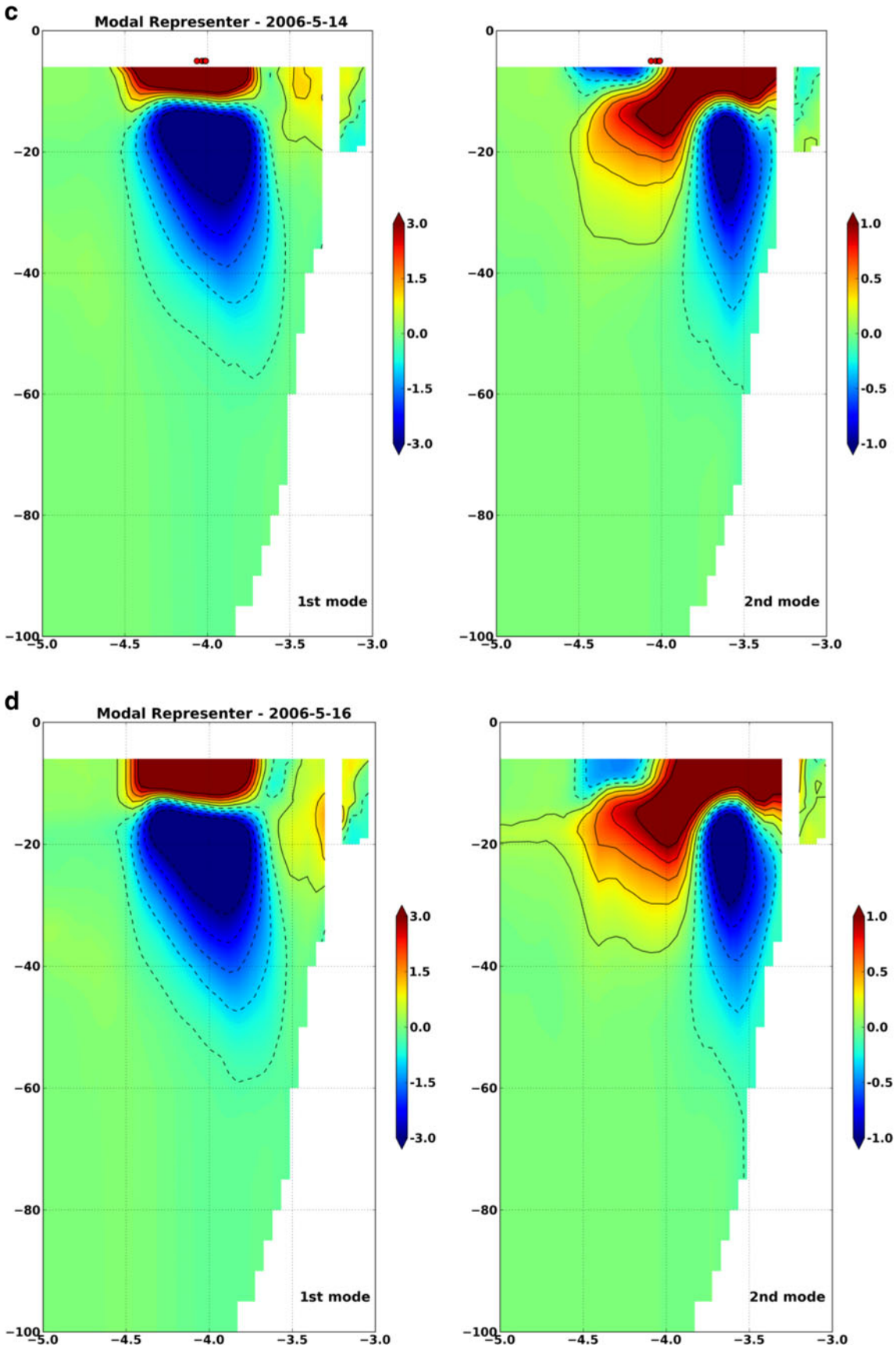

Fig. 10 continued.

4.3 Extension of the analysis to the other seasons

Under winter, summer and autumn conditions, the same protocol, as defined in Section 4.1, has been applied. A synthesis of the main results is provided in the following section.

4.3.1 Model error subspace

By nature, the model sensitivity to the different perturbed parameters (as a reminder: the atmospheric forcing, the bottom-friction coefficient, the turbulence-closure coefficient and the light extinction coefficient) is linked to the water column stratification conditions and the river outflow regimes. As a result, the distribution of the model uncertainties appears to vary both seasonally and spatially.

In winter, the 4D (longitude, latitude, time, depth) ensemble variance is generally small (lower than 0.15 °C) except in the vicinity of main rivers (Seine, Loire, Gironde, and Adour) where the error amplitude ranges from 0.2 to 0.4 °C. These limited-extension cells of uncertainty are mainly generated by the perturbations in the turbulence-closure coefficient and the atmospheric forcings. During this period, no significant error structure is actually sampled, since (1) only a few profiles are available and (2) those profiles are not located in the error cells associated with uncertainties in the river's plume dynamics (not shown).

During the summer, the maximal ensemble dispersion is mainly localized in the first 40 m of the water column over the Bay of Biscay shelves and in the western English Channel in the vicinity of the Ushant front. In those areas, the model error is about 0.4 °C. A total of 131 profiles is available to sample the model error subspace. Those profiles are distributed amongst three sets (Fig. 12): in the eastern English Channel (set no. 1), in the western English Channel close to the Ushant front (set no. 2) and over the Armorican shelf in south of Brittany (set no. 3). Set no. 1 does not sample any significant error structures, while set no. 2 provides an efficient detection of the model error structures that grow in this area; in particular, the 20-m-depth error layer is accurately detected by these profiles. Set no. 3 covers the whole studied period, and the associated profiles are adequately scattered in space and time to be able to detect the growth of model uncertainties in this area.

Finally, in autumn, the model error structures appear to be more heterogeneous than during the other seasons. At the surface, uncertainties are mainly located above the continental slope and the abyssal plain. The 106 profiles available during the period do not sample any significant model error structures, except for a few profiles over the Armorican shelf (not shown).

4.3.2 ArM analysis

The representer matrix spectrum, presented in Fig. 8 for the four analysed periods, clearly confirms that the performances of a RECOPESCA network are related to the spatiotemporal profile distribution. Better performances are associated with networks including wider spatiotemporal profile distribution. Indeed, in winter, the seven poorly located profiles do not allow to detect any error modes (all eigenvalues are lower than 1). On the other hand in spring, summer and autumn, the number of profiles, as well as their space-time dissemination, are more favourable. In those configurations, the network allows the detection of 22 and 29 model error modes (amongst the 50 detectable), respectively, in autumn and in spring/summer.

In summer and autumn, the first mode dominates (44 and 56 % of the explained variance, respectively). The second and third modes are closer in terms of representativeness with smaller explained variances (13.5 and 11 % for the second and third mode in autumn, and 20 and 9 % in summer). Regarding the associated modal representers, the first, second and third ones are, respectively, associated with 26, 14 and 41 modal profiles amongst the 131 available profiles in summer. In autumn, the ratio is of 21, 27 and 29 modal profiles over the whole population of 106 available profiles. Based on the dedicated efficiency diagnostic, the RECOPESCA network appears to be slightly more efficient in autumn rather than in summer, since the ratio of the "modal profile population" over the "whole profile population" is larger in autumn.

Furthermore, the space-time distribution of the modal profiles over the modal representers (Fig. 13) can give an insight into the network ability to detect some model error structures in a privileged way: for instance, in summer, one can notice that the modal profile population associated with the first mode (Fig. 13a) detects the well-established structures over the Armorican shelf, while modal profiles associated with the second mode (Fig. 13b) constrain the more variable error structures in the western English Channel. This distinction can be explained by the fact that the model error growth in the western English Channel is characterized by a larger space-time variability than the one over the Armorican shelf; thus, the network would detect at first these "stationary" error structures on Armorican shelf then detect the more variable error cells in the western English Channel.

5 Extension scenarios

5.1 Introduction

In the first part of the study, the ArM method was implemented to assess the performances of the RECOPESCA network in its reference configuration. This configuration was based on a

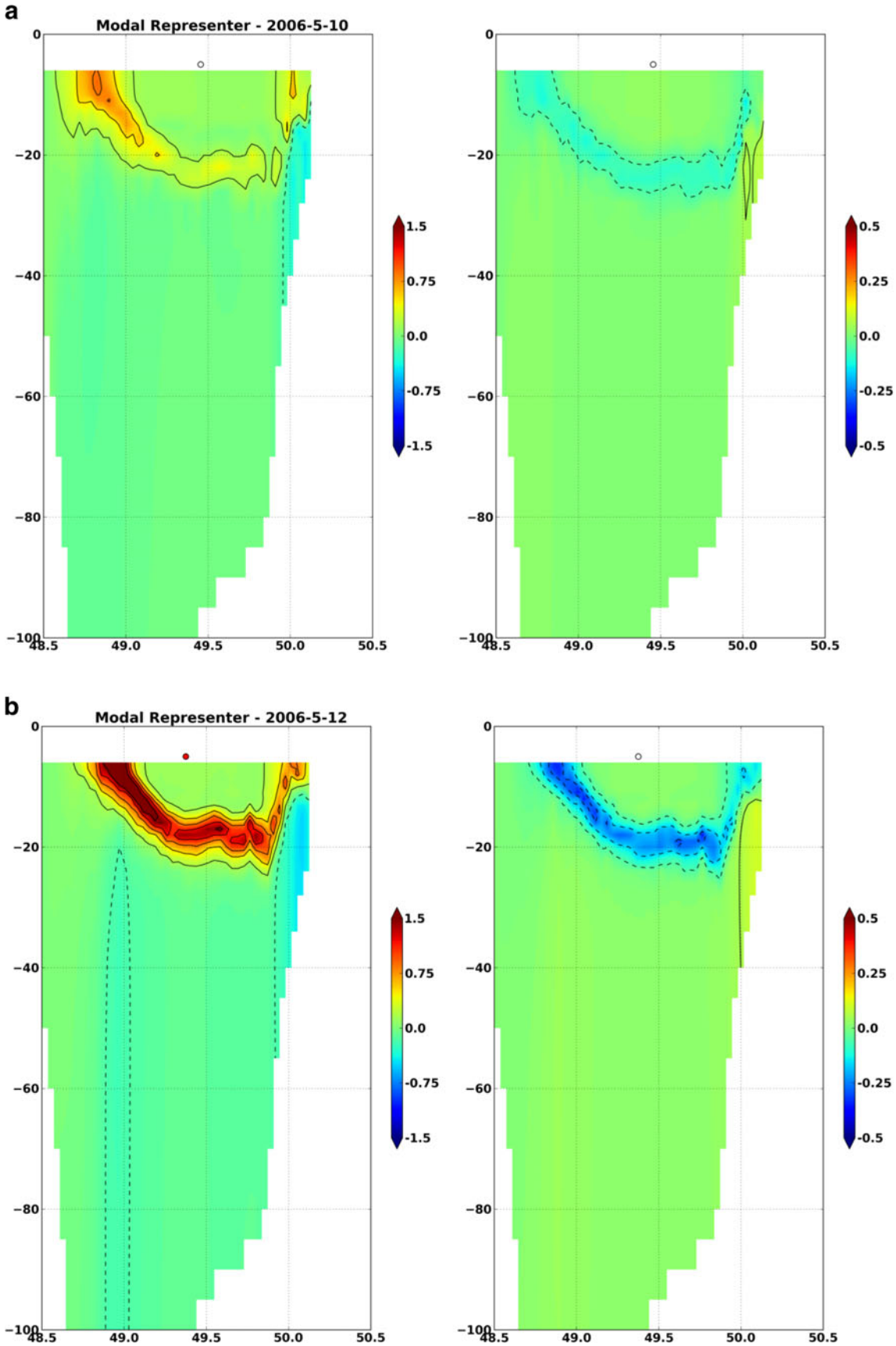
a
Modal Representer - 2006-5-10
0
−20
−40
−60
−80
−100
48.5
49.0
49.5
50.0
50.5
1.5
0.75
0.0
-0.75
-1.5
0.5
0.25
0.0
-0.25
-0.5
b
Modal Representer - 2006-5-12

◀ **Fig. 11** North-South vertical section of the first and second modal representers for (**a**) 10, (**b**) 12, (**c**) 14, and (**d**) 16 May 2006, at 5° W in the western English Channel (unit: °C)

set of temperature profiles collected during the year 2008. Although the general performances of this reference network appear to be satisfying and promising, some lacks have been highlighted in the spatiotemporal distribution of the winter and autumn sets of profiles. We thus explore in this section the contributions of two extension scenarios for the reference RECOPESCA network. Note that the analysis protocol is the same as the one applied in Section 4.1, i.e. based on the detection and the analysis of the degrees of freedom of the model error subspace. Nevertheless, for clarity reasons, the focus will be on the spring season, while synthetic results will be provided for the other seasons.

5.2 Description of the extension scenarios

The extension scenarios are displayed in Fig. 14. The first extension scenario (hereafter "SC1") is based on the set of profiles sampled during the year 2010; the second one (hereafter "SC2") is built on the collection of profiles sampled during the years 2006 to 2011. This collection reflects an expected coverage in a near. A first overview shows that the number of measured profiles has been strongly increased with respect to the reference scenario. The space-time sampling is also extended, even if the locations of the profiles remain limited to the continental shelf, since they depend on the localization of the RECOPESCA vessel's fishing areas.

5.3 Detailed results

5.3.1 Spring period

In spring, the SC1 network is composed of 296 profiles mainly distributed between three sets (Fig. 14): a first one is localized on the Celtic Shelf (cf. Fig. 1), a second one on the edge of the Celtic slope and the last one over the Armorican shelf. Two smaller groups of profiles can also be identified in the middle of the English Channel, and near the Gironde river mouth. The SC2 network comes with 883 profiles, split up into six sets (Fig. 14): on the Celtic shelf, near the Celtic slope, in the eastern English Channel, in the western part of the English Channel, over the Armorican shelf and close to the Landes coasts (on Aquitaine shelf).

During this spring period, the model error growth is mainly localized on the French continental shelf and in the western English Channel (Fig. 15). The SC1 profiles are thus able to mainly sample the model error structures that develop over the Armorican shelf and near the Gironde river mouth. The amplitude of these "observed" model errors is about 0.3 °C. The wider spatiotemporal distribution of the SC2 allows observing not only the model error growth over the French Continental shelf but also the model error structures that develop in the west English Channel.

Figure 16 displays the representer matrix spectrum for the reference, SC1 and SC2 networks. Both SC1 and SC2 networks come with performances (in terms of model error mode detection) greater than the reference one: they can detect, respectively, 45 and 49 d.o.f. amongst the 50 detectable ones, while the reference network can only detect 29 d.o.f.

The performances of the SC2 network are larger than those associated with the SC1 network: if the number of d.o.f. detected by both networks is rather similar (45 vs 49), the total spectrum energy of the SC2 network is higher than the one associated with SC1 network, since all SC2 spectrum eigenvalues are larger than of the SC1 spectrum. It is thus likely that the SC2 network could detect additional error modes when the rank of the system exceeds 50. Increasing the number of model ensemble simulations would thus enhance the capability of the methodology to discriminate networks.

Comparing with the reference network, the spectrum of both extended networks is more distributed between all the modes, since there is no significantly dominant mode. We expect here that secondary modes should bring relevant information.

The SC1 and SC2 networks are compared to the reference one through their respective modal profiles. We note about these following modal profiles (not shown) that:

1. All the SC1 modal profiles are localized over the Armorican shelf, while the SC2 ones are distributed between the Armorican shelf and the western English Channel. Indeed, it has been shown that the SC2 network is able to detect the model error growth in the western English Channel, where the SC1 network does not sample this area.
2. The SC2 first representer comes with at least four times more modal profiles than the SC1 network (296 against 34), whereas the total number of SC2 profiles is less than three times the total number of SC1 ones (883 against 212); besides the comparison of the spectra, this confirms that the SC2 network efficiency (0.24) is higher than the SC1 one (0.11) regarding the detection of the model error modes.

Regarding the studied spring period, the SC2 scenario appears to be more efficient than the reference and SC1 networks to detect the model error modes under consideration.

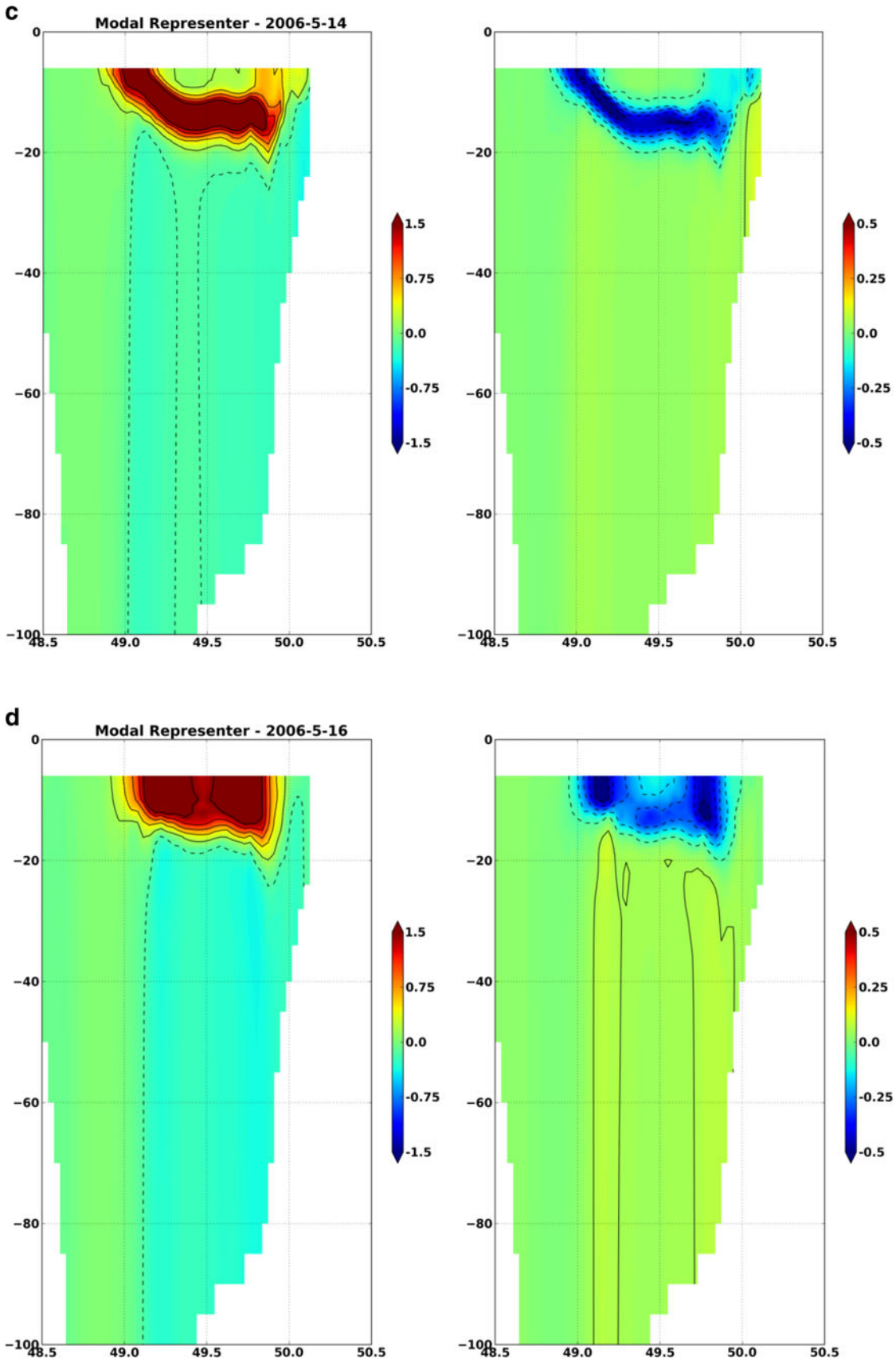

Fig. 11 continued.

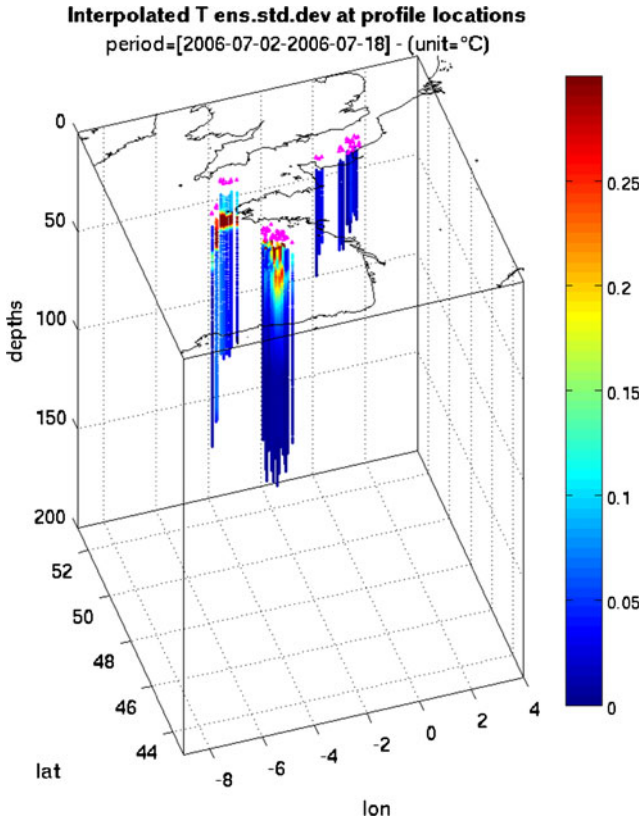

Fig. 12 Model error space-time interpolated on profile locations. Position in surface (*pink triangles*) and at depth (*coloured dots*) from July 4 to 18 July 2006

5.3.2 Synthetic results for other seasons

For clarity reasons, the synthesis of the reference and extension configuration cross-comparison has been restricted to the analysis of (1) the representer matrix spectrum and (2) the efficiency-oriented diagnostics associated with the three configurations under consideration.

Analysis of the representer matrix spectrum Figure 17 displays the representer matrix spectrum associated with the reference and both extension configurations, for the winter, summer and autumn periods. As for the spring period, the performances in terms of model error mode detection appear higher for both extended networks. Globally, the SC1 and SC2 configurations allow to detect more model error modes than the reference scenario. This result confirms that increasing the space-time coverage of the RECOPESCA profile population is associated with better performances in terms of model error detection. Nevertheless, during all seasons, the SC2 network shows a larger number of detected error modes with a limitation due to the rank of the system in summer. This limited rank thus acts as a limitation of the capability of the methodology to discriminate between both extended configurations, using that criterion.

Efficiency-oriented analysis In order to give a complementary insight of the extension scenario performances, Table 1 gathers the efficiency values associated with the reference and both extension configurations, for the three studied periods.

The efficiency indicator provides another point of view on the various network configuration performances. It appears that increasing the number of profiles does not necessarily result in greater efficiency. Indeed, since all the additional profiles are not de facto scattered in an optimal way, the number of modal profiles is not proportional to the whole profile populations. In that context, it is likely that a trade-off can be found between the number of profiles from the extended SC1 and SC2 networks, to ensure the optimal detection and description of model error modes. Based on this indicator, we can also notice that for all seasons, the reference network appears as more efficient than the scenario SC1.

5.4 Conclusions on the extension scenarios

Two extended versions of the reference configuration network have been explored in this section. The first extension scenario (SC1) is based on temperature profiles sampled during the year 2010. The second extension configuration (SC2) is a collection of all available profiles during the period 2006–2011. Considering the

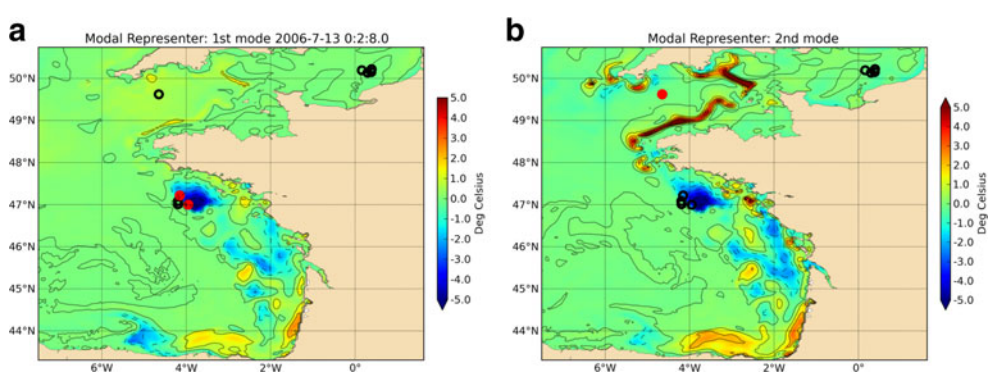

Fig. 13 First (**a**) and second (**b**) modal representers (6-m-depth horizontal section) for July 13, 2006. Location of the profiles (*black circles*) and the modal profiles (*red spots*) at this date

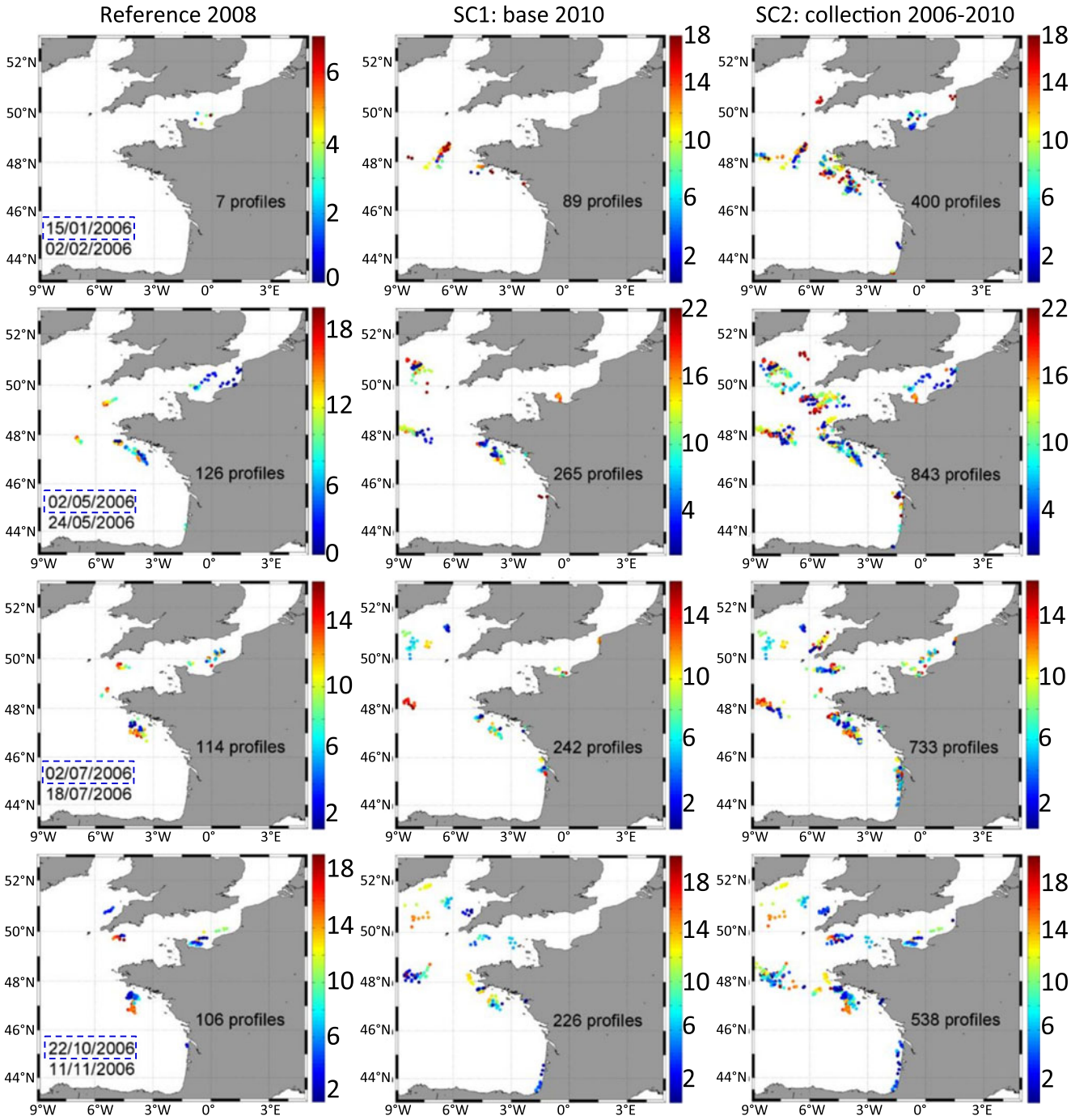

Fig. 14 Location of RECOPESCA profiles for the reference configuration (*left*), the 2010 scenario (*centre*) and the 2006–2011 scenario (*right*), for the winter (*row 1*), spring (*row 2*), summer (*row 3*) and autumn (*row 4*) periods. Unit: elapsed days since the first day of each period (this date is highlighted in the *blue dashed rectangle*)

whole studied periods, the extension scenarios logically provide better performances than the reference one, thanks to their wider and denser spatiotemporal coverage of the area. During the spring, summer and autumn periods, where the reference network already has satisfying detection ability, the network extension allows a better capture and description of the model error subspace variability modes. As to the tricky winter period, where the model error growth is very episodic and limited in space, the extended networks provide a drastic enhancement of the detection performances, whereas the reference network is not able to sample any significant model error growth (the efficiency indicator is not relevant for this season as the number of profiles is very small).

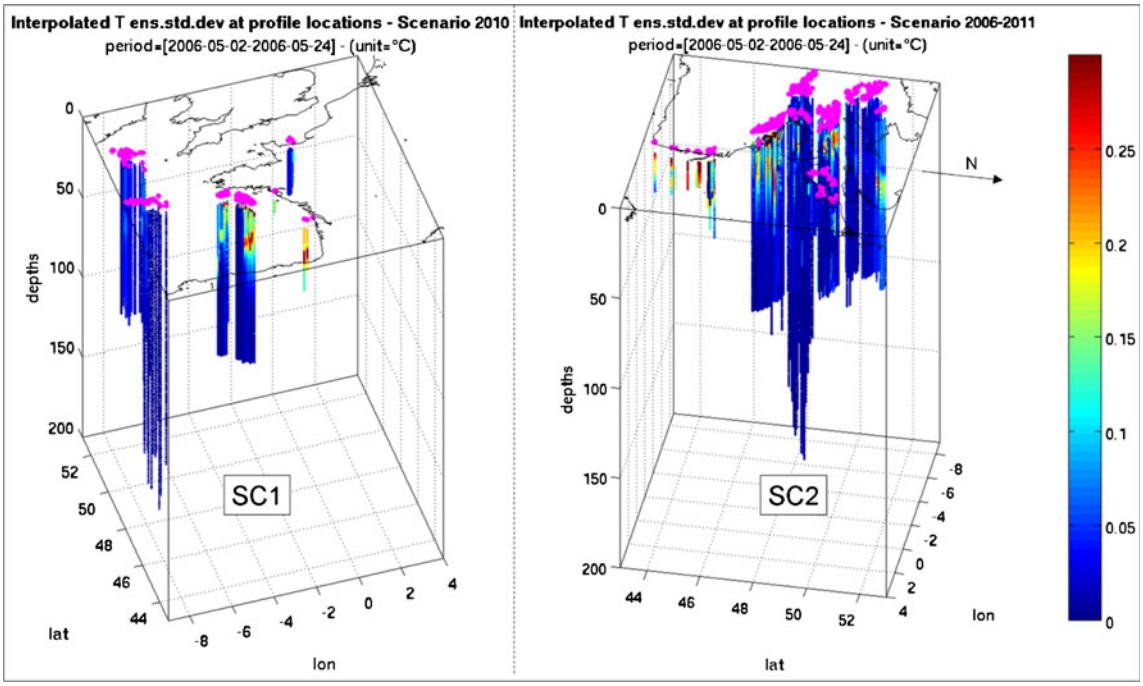

Fig. 15 Model space-time interpolated error on profile locations of the SC1 network (*left*) and the SC2 network (*right*)—position at surface (*pink triangles*) and at depth (*coloured dots*) from May 3 to 25, 2006

When it comes to the comparison between both extended configurations, the SC2 network appears to be more efficient than the SC1 extended configuration, not only in terms of the number of detected modes but also through the ability to accurately describe the model error structures. Moreover, regarding the number of profiles, the SC2 network has been shown to provide more efficient profiles than the SC1 one, in significant proportions. Eventually, it has been highlighted that the rank of the system, imposed by the dimension of the ensemble of perturbed simulations, has been reached in two cases of study (spring and summer periods) for the SC2 network detection ability. This limited rank was thus acting as a limitation to the capability of the methodology to discriminate between both extended configurations, using the criterion based on the representer matrix spectrum analysis. Hence, it is likely that increasing the number of perturbed simulations, and thus

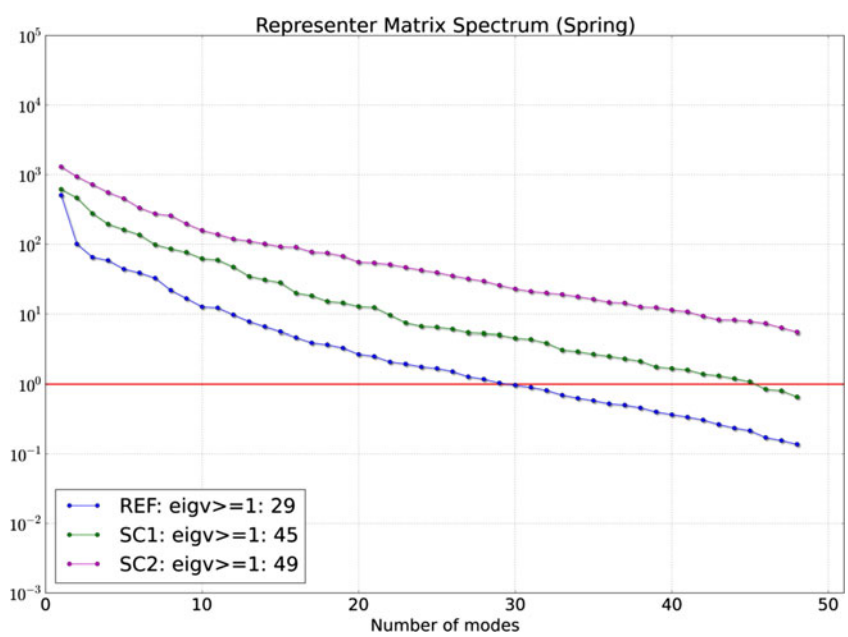

Fig. 16 Representer matrix spectrum relative to the reference network (*blue*), the SC1 network (*green*) and the SC2 network (*pink*) for the period from May 3 to the 25, 2006

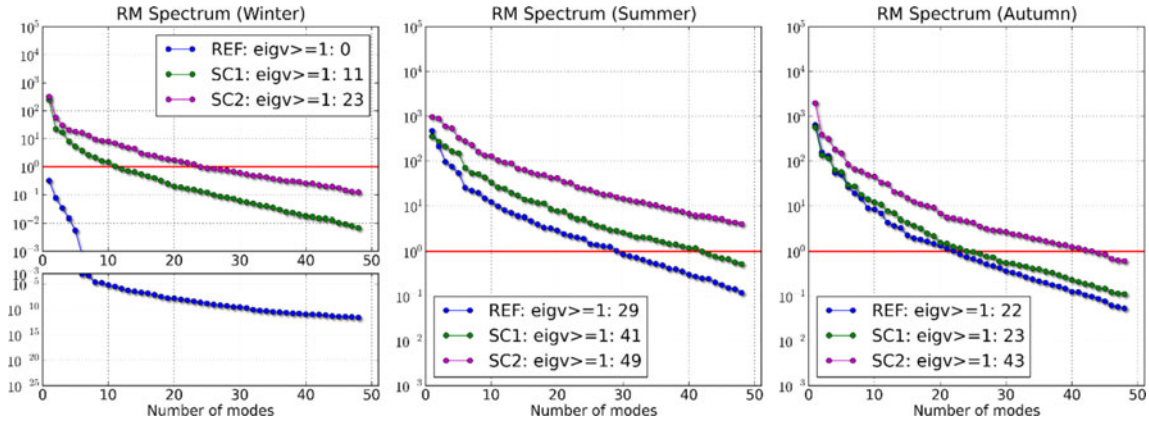

Fig. 17 Representer matrix spectra relative to the reference (*blue*), the SC1 (*green*) and the SC2 (*pink*) networks for the winter (*left*), summer (*middle*) and autumn (*left*) periods under consideration. In winter, the *top figure* is representing a zoomed spectrum for values between 10^{-3} and 10^{5}, and the *bottom figure* is the second part of the spectrum for small values (between 10^{-25} and 10^{-3}) covering a larger range of values

refining the model error subspace approximation, will enhance the network discrimination.

6 Conclusions

The present study aims at (1) investigating and assessing the RECOPESCA network ability to detect a number of realistic modes of uncertainty as stochastically simulated in the Bay of Biscay and English Channel temperature dynamics and (2) comparing on qualitative and quantitative ground several observational scenarios in an attempt to guide the future operation of the RECOPESCA programme.

At low computational cost, the use of the ArM method for helping design and guide improvements of the observation network, indeed, allows exploring the model error subspace and highlighting major group of profiles that can constrain these uncertainty cells. Analysing the results for the various seasons, we conclude that the reference network (based on the 2008 profile distribution) is efficient for most of the year, except in winter when there are too few observations. In the latter case, the ArM method highlights strengths and weaknesses of the RECOPESCA network. Indeed, the added value of a sustainable network based on fishing vessels of opportunity is confirmed by the efficiency of this collection of profiles at detecting the main modes of variability in this region.

Table 1 Efficiency-oriented diagnostic—relative to the dominant detected model error mode—associated with the reference and both extension configurations, for the winter, summer and autumn periods

Efficiency	REF	SC1	SC2
Winter	0.14[a]	0.03	0.09
Spring	0.23	0.11	0.24
Summer	0.20	0.19	0.20
Autumn	0.20	0.10	0.15

[a] No detected model error mode for this configuration (cf. Fig. 17)

These results are based on a given observation error (0.3 °C) that can be further discussed depending on local features. However, sensitivity tests confirm that the present assessment remains valid with different observation errors. Changes in these errors will translate the spectra to higher (lower) values if observation errors are larger (smaller) influencing the number of detected modes. Then, comparisons between different seasons/scenari will remain similar as well as spatiotemporal structures of representers.

A few suggestions regarding possible observation network extensions can be drawn from the present study. The scenario exploration pointed out the importance of the sampling of key regions in the Bay of Biscay and the English Channel to constrain model uncertainties and by extension, to monitor regions of large physical variability. The need to keep collecting profiles in the western English Channel has been confirmed. Also, the number of profiles cannot be considered as a valid unique indicator of efficiency (cf. scenario SC2). These recommendations have been taken into account for future evolutions of the equipped fishing vessels.

RECOPESCA programme is also collecting salinity profiles with some fishing vessels. The multi-parameter assessment would be considered as soon as the quality and the number of salinity profiles will be suitable for the exploration. However, linked to the river-driven dynamics in the region, we anticipate similar conclusions considering temperature and salinity profiles.

This study illustrates the potential benefit of the existing French network HOSEA (High frequency Observation network for the environment in coastal SEAs) which is supporting a sustainable RECOPESCA network in the Bay of Biscay and the English Channel as

a key component of the continental shelf (including outer shelf) observing systems for research and operational oceanography. Further studies (Charria et al. 2015) are investigating the complementary local use of other profiling autonomous systems like gliders and of other variables (e.g. salinity).

Acknowledgments This study has been undertaken in the frame and with the financial support of the PREVIMER project, the FP7 JERICO (WP9) project, and the FP7 SANGOMA project (FP7-SPACE-2011-283580). M. Le Hénaff received partial support for this work from the base funds of the NOAA Atlantic Oceanographic and Meteorological Laboratory. It has also been conducted as a contribution to the GODAE OceanView Coastal Ocean and Shelf Seas Task Team (COSS-TT). We would like to thank Emilie Leblond and Patrick Berthou for leading the RECOPESCA programme, Loic Quemener and Michel Repecaud for operating the network, and the voluntary fishermen who have accepted to join the RECOPESCA network. We also thank the technical team of RECOPESCA, especially Matthieu Bourbigot, and the observers of the Ifremer Fisheries Information System. The data from the EUMETSAT Satellite Application Facility on Ocean and Sea Ice is accessible through the SAF's homepage: http://www.osi-saf.org. We are grateful to the two anonymous referees and the Associate Editor Emil Vassilev Stanev for their very fruitful and constructive comments on this manuscript.

References

Alvarez A, Mourre B (2014) Cooperation or coordination of underwater glider networks? An assessment from Observing System Simulation Experiments in the Ligurian Sea. J Atmos Oceanic Tech 31:2268–2277. doi:10.1175/JTECH-D-13-00214.1

Auclair F, Marsaleix P, de Mey P (2003) Space-time structure and dynamics of the forecast error in a coastal circulation model in the Gulf of Lions. Dyn Atmos Oceans 36(4):309–346

Bennett AF (1985) Array design by inverse methods. Prog Oceanogr 15: 129–151

Bennett AF (1990) Inverse methods for assessing ship-of-opportunity networks and estimating circulation and winds from tropical expendable bathythermograph data. J Geophys Res 95:16111–16148

Buizza R (2006) The ECMWF ensemble prediction system. In: Predictability of weather and climate, 17. Cambridge University Press, p. 459–488

Charria G, Lazure P, Le Cann B, Serpette A, Reverdin G, Louazel S, Batifoulier F, Dumas F, Pichon A, Morel Y (2013) Surface layer circulation derived from Lagrangian drifters in the Bay of Biscay. J Mar Syst. 109–110:S60-S76. ISSN 0924-7963. 10.1016/j.jmarsys.2011.09.015

Charria G, Repecaud M, Quemener L, Ménesguen A, Rimmelin-Maury P, L'Helguen S, Beaumont L, Jolivet A, Morin P, Macé E, Lazure P, Le Gendre R, Jacqueline F, Verney R, Marié L, Jegou P, Le Reste S, André X, Dutreuil V, Regnault JP, Jestin H, Lintanf H, Pichavant P, Retho M, Allenou JA, Stanisière JY, Bonnat A, Nonnotte L, Duros W, Tarot S, Carval T, Le Hir P, Dumas F, Vandermeirsch F, Lecornu F (2014) PREVIMER: a contribution to in situ coastal observing systems. Q Newslet MERCATOR Ocean 49

Charria G, Lamouroux J, De Mey P (2015) Optimizing observation networks using gliders, moored buoys and FerryBox in the Bay of Biscay and English Channel. Submitted to Journal of Marine Systems

Cuypers Y, Bouruet Aubertot P, Lazure P, Lourenço A, Lunven M, Sourisseau M, Velo-Suarez L (2011) Non linear internal tides, turbulent mixing in the continental shelf of South Brittany. EPIGRAM Annual Meeting. Ile de Ré

Duhaut T, Honnorat M, Debreu L (2008) Développements numériques pour le modèle MARS. Rapport PREVIMER contrat N06/2 210 290

EUMETSAT (2006) Atlantic sea surface temperature product manual. http://www.osi-saf.org/biblio/docs/ss1_pmatlsst_1_6.pdf

Ferrer L, Fontán A, Mader J, Chust G, González M, Valencia V, Ad U, Collins MB (2009) Low-salinity plumes in the oceanic region of the Basque Country. Cont Shelf Res 29(8):970–984

Friedrichs MAM (2001) A data assimilative marine ecosystem model of the central equatorial Pacific: numerical twin experiments. J Mar Res 59:859–894

Halliwell GR, Srinivasan A, Kourafalou V, Yang H, Willey D, Le Hénaff M, Atlas R (2014) Rigorous evaluation of a fraternal twin ocean OSSE system in the open Gulf of Mexico. J Atmos Ocean Technol 31(1):105–130. doi:10.1175/JTECH-D-13-00011.1

Heyraud C (2011) Assimilation de Données dans les modèles de façade. Ensemble de Prévisions. Années 2006, 2008. Report 11.20. Actimar.

Huret M, Gohin F, Delmas D, Lunven M, Garçon V (2007) Use of SeaWIFS data for light availability and parameter estimation of a phytoplankton production model of the Bay of Biscay. J Mar Syst 65:509–531

Ide K, Courtier P, Ghil M, Lorenc A (1997) Unified notations for data assimilation: operational, sequential and variational. J Meteorol Soc Jpn 75(1B):181–189

Isemer HJ, Hasse L (1985) The Bunker climate atlas of the North Atlantic Ocean, vol 2. Springer, Berlin, pp 218–252

Lazure P, Dumas F (2008) An external-internal mode coupling for a 3D hydrodynamical model for applications at regional scales (MARS). Adv Water Resour 31(2):233–250. doi:10.1016/j.advwatres.2007.06.010

Lazure P, Jegou AM (1998) 3D modelling of seasonal evolution of Loire and Gironde plumes on Biscay Bay continental shelf. Oceanol Acta 21(2):165–177

Lazure P, Jegou AM, Kerdreux M (2006) Analysis of salinity measurements near islands on the French continental shelf of the Bay of Biscay. Sci Mar 70(S1):7–14

Le Boyer A, Cambon G, Daniault N, Herbette S, Le Cann B, Marié L, Morin P (2009) Observations of the Ushant tidal front in September 2007. Cont Shelf Res 29(8):1026–1037. doi:10.1016/j.csr.2008.12.020

Le Hénaff M, De Mey P, Marsaleix P (2009) Assessment of observational networks with the representer matrix spectra method—application to a 3d coastal model of the Bay of Biscay. Ocean Dyn 59:3–20. doi:10.1007/s10236-008-0144-7

Lea DJ, Martin MJ, Oke PR (2014) Demonstrating the complementarity of observations in an operational ocean forecasting system. Q J Roy Meteorol Soc 140:2037–2049. doi:10.1002/qj.2281

Leblond E, Lazure P, Laurans M, Rioual C, Woerther P, Quemener L, Berthou P (2010) RECOPESCA: a new example of participative approach to collect in-situ environmental and fisheries data. Joint Coriolis–Mercator Ocean Quarterly Newsletter 37

Mourre B, Ballabrera-Poy J (2009) Salinity model errors induced by wind stress uncertainties in the Macaronesian region. Ocean Model 29(3): 213–221. ISSN 1463–5003. 10.1016/j.ocemod.2009.05.002

Mourre B, De Mey P, Lyard F, Le Provost C (2004) Assimilation of sea level data over continental shelves: an ensemble method for the exploration of model errors due to uncertainties in bathymetry. Dyn Atmos Oceans 38:93–121. doi:10.1016/j.dynatmoce.2004.09.001

Pairaud IL, Lyard F, Auclair F, Letellier T, Marsaleix P (2008) Dynamics of the semi-diurnal and quarter-diurnal internal tides in the Bay of Biscay. Part 1: barotropic tides. Cont Shelf Res 28(10):1294–1315

Pairaud IL, Auclair F, Marsaleix P, Lyard F, Pichon A (2010) Dynamics of the semi-diurnal and quarter-diurnal internal tides in the Bay of Biscay. Part 2: baroclinic tides. Cont Shelf Res 30(3):253–269

Pichon A, Correard S (2006) Internal tides modelling in the Bay of Biscay. Comparisons with observations. Sci Mar 70(S1):65–88

Pingree RD, Le Cann B (1989) Celtic and Armorican slope and shelf residual currents. Progr Oceanogr 23(4):303–338

Pingree RD, Le Cann B (1990) Structure, strength and seasonality of the slope currents in the Bay of Biscay region. J Mar Biol Assoc UK 70: 857–885

Quattrocchi G, De Mey P, Ayoub N, Vervatis V D, Testut C E, Reffray G, Chanut J, Drillet Y (2014) Characterisation of errors of a regional model of the Bay of Biscay in response to wind uncertainties: a first step toward a data assimilation system suitable for coastal sea domains. J Oper Oceanogr 7(2)

Sakov P, Evensen G, Bertino L (2010) Asynchronous data assimilation with the EnKF. Tellus A 62(1):24–29. doi:10.1111/j.1600-0870.2009.00417.x

Xie XH, Cuypers Y, Bouruet-Aubertot P, Ferron B, Pichon A, Lourenço A, Cortes N (2013) Large-amplitude internal tides, solitary waves, and turbulence in the central Bay of Biscay. Geophys Res Lett 40: 2748–2754. doi:10.1002/grl.50533